DAMAGE PROGRESSION IN BUCKLE-RESISTANT NOTCHED COMPOSITE PLATES LOADED IN UNIAXIAL COMPRESSION

David M. McGowan, Carlos G. Dávila, and Damodar R. Ambur
NASA Langley Research Center
Hampton, VA 23681-2199

Presented at the 42nd AIAA/ASME/ASCE/AHS/ASC
Structures, Structural Dynamics and Materials Conference
Session No. 37 – Durability and Damage Tolerance

AIAA Paper No. 2001-1482

Seattle, Washington
April 16-19, 2001

AIAA 2001-1482

DAMAGE PROGRESSION IN BUCKLE-RESISTANT NOTCHED COMPOSITE PLATES LOADED IN UNIAXIAL COMPRESSION

David M. McGowan*, Carlos G. Dávila†, and Damodar R. Ambur‡
NASA Langley Research Center
Hampton, VA 23681-2199

Abstract

Results of an experimental and analytical evaluation of damage progression in three stitched composite plates containing an angled central notch and subjected to compression loading are presented. Parametric studies were conducted systematically to identify the relative effects of the material strength parameters on damage initiation and growth. Comparisons with experiments were conducted to determine the appropriate *in situ* values of strengths for progressive failure analysis. These parametric studies indicated that the *in situ* value of the fiber buckling strength is the most important parameter in the prediction of damage initiation and growth in these notched composite plates. Analyses of the damage progression in the notched, compression-loaded plates were conducted using *in situ* material strengths. Comparisons of results obtained from these analyses with experimental results for displacements and axial strains show good agreement.

Introduction

Stitched graphite-epoxy structures have demonstrated a potential for reducing the weight and the cost of future commercial transport aircraft. Under the sponsorship of the NASA Advanced Subsonics Technology (AST) Composite Wing Program, the Boeing company (formerly McDonnell Douglas) has developed an automated process to stitch entire wing cover panels together, including skins, stringers, and spar caps. The stitched structure is then infused with epoxy resin using the Resin Film Infusion (RFI) process.[1] The combined manufacturing process is referred to herein as Stitched/Resin Film Infusion (S/RFI). The S/RFI process eliminates the need for most fasteners and reduces both the cost and the weight of the structure. One of the requirements for the development and application of composite primary structures is the demonstration of structural damage tolerance with a two-stringer-bay-wide notch. The response of notched wing panels made of stitched material and loaded in compression or tension is not well understood. There is a need for experimentally validated analysis methods to predict the damage initiation and growth at the notch. Such analysis methods can eventually be used to predict the residual strength of stitched composite primary structures.

The objective of the present work is to study local damage-growth prediction methods and the effect of damage on the response and residual strength of stitched graphite-epoxy plates with centered notches oriented at different angles with respect to an axial compression loading direction. These plates are representative of the structure that has been used in the upper cover panel of an advanced composite civil transport wing manufactured by Boeing as part of AST Composite Wing program.[2] A complete description of an earlier stitched graphite-epoxy wing stub box fabricated by Boeing and the tests that were conducted on this wing box at NASA Langley Research Center can be found in Ref. 3. The flat plates used for the present study were manufactured at NASA Langley Research Center.

The progressive damage analysis method used in the present study was presented in Ref. 4, and used to predict the extent of the local damage and the failure modes as a function of the applied load in notched wing cover panels machined from the wing stub box described in Ref. 3. This analysis model is based on superposed shell elements, which is a useful technique to reduce the number of integration points through the thickness. Bending effects on damage growth are also considered by using multiple independent integration points through the thickness of the laminate. The effect

*Aerospace Engineer, Structural Mechanics Branch. Senior Member, AIAA.

†Aerospace Engineer, Analytical & Computational Methods Branch.

‡Head, Mechanics and Durability Branch. Associate Fellow, AIAA.

of the stitching is modeled by applying a stitching scale factor, *SF*, to the fiber-buckling strength value of the rows of elements corresponding to the location of the stitch lines. As stated previously and discussed subsequently, the method of Ref. 4 uses superposed shell elements with each shell element representing the total number of plies in the laminate of a given orientation. Therefore, in thick laminates such as those used in the present study, the failure criteria are interrogated at multiple integration points through the thickness for a small number of individual shell elements (i.e., ply orientations). Ply discounting is then used to reduce the properties of each shell element that exhibits failure.

The present paper describes an experimental and analytical evaluation of damage progression in three composite plates containing a central notch that is oriented at an angle α to the direction of the applied uniaxial compression loading. The progressive failure analysis methodology of Ref. 4 is also described briefly. Comparisons between predicted and measured strains and displacements are presented. The analytical results are in good agreement with the experimental results. The analyses indicate that the nominal value of the fiber buckling allowable may be too low to adequately represent the local response in the presence of a notch. The analyses also indicate that local stitching increases the compression damage tolerance of the material by delaying fiber buckling.

Description Of Test Plates, Test Apparatus, And Test Conditions

The three composite plates studied in the present paper were fabricated from material that is representative of the upper cover panels of a 40-foot-long, S/RFI graphite-epoxy wing box manufactured by Boeing as part of the NASA AST Composite Wing Program.[2] A brief description of the materials used to fabricate the three test panels is given here. The test plates were machined from a larger panel that was fabricated using Hercules, Inc. AS4/3501-6 graphite-epoxy materials that were stitched together using E.I. DuPont de Nemours, Inc. Kevlar® thread. The larger panel was fabricated from prekitted "stacks" of nine layers of dry graphite material forms. Each prekitted "stack" of material is approximately 0.055-inches thick and has a $[45, -45, 0_2, \overline{90}]_s$ laminate stacking sequence. The cured thickness of each of the plies is 0.00590, 0.00618, and 0.00668 inches for ±45, 0, and 90-degree orientations, respectively. The dry preform of the panel was fabricated by stitching ten "stacks" of material together to provide the desired thickness. Resin is infused into the panel using the Resin Film Infusion (RFI) process described in Ref. 1.

A schematic representation of the test plates is shown in Fig. 1. The plates are each 9.0-inches wide and 12.0-inches long. A 3/16-in.-wide, 3.0-in.-long notch oriented at an angle α to the direction of the applied axial compression load was machined at the center of each plate. The values of α considered in the present study are 45°, 60°, and 90°. The plates containing notches of these orientations will be referred to herein as P-45, P-60, and P-90. The nominal thickness of the panels is 0.55 inches. The nominal material properties and ply thickness fraction of each ply orientation for the material used in the test plates is presented in Table 1.

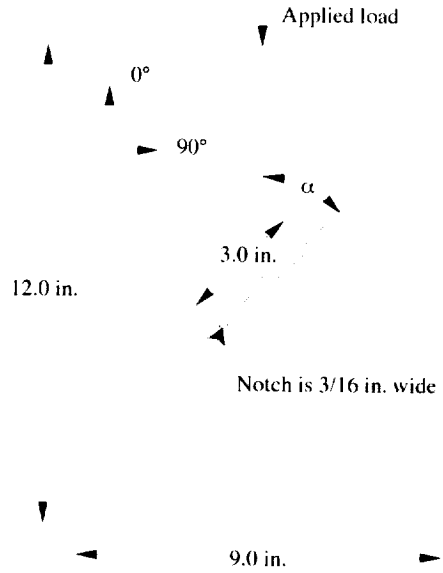

Fig. 1. Schematic representation of a stitched, graphite-epoxy plate with a central, machined notch.

Table 1. Material properties and ply thickness fractions for each ply orientaion of the test plates

Property	Ply orientation		
	±45°	0°	90°
E_L (Msi)	16.15	16.43	15.97
E_T (Msi)	1.60	1.60	1.60
G_{LT} (Msi)	0.8	0.8	0.8
ν_{LT}	0.34	0.34	0.34
Thickness fraction	0.2147	0.4491	0.1214

Uniaxial compression loading was applied to the 9.0-in.-wide edges of the plates. These loaded edges were machined flat and parallel to each other to assure that a

uniform loading was applied to the plates. The loaded ends of the plates were clamped to a depth of 0.625 in. by a steel loading fixture to prevent an end-brooming failure. Knife-edge supports were used to support the unloaded edges of the plate to provide a simple support boundary condition along those edges and to prevent premature wide-column plate buckling. Surface strains were measured using electrical resistance strain gages, and displacements were measured using differential current displacement transducers (DCDT's).

A photograph of the test set-up for plate P-90 is given in Fig. 2(a). The steel loading fixture, knife-edge supports and DCDT's used to measure end shortening are indicated in this figure. A photograph showing the locations of the strain gages in the vicinity of one of the notch tips of plate P-90 is shown in Fig. 2(b). This photograph also shows the stitch lines, with a spacing of 0.2 inches.

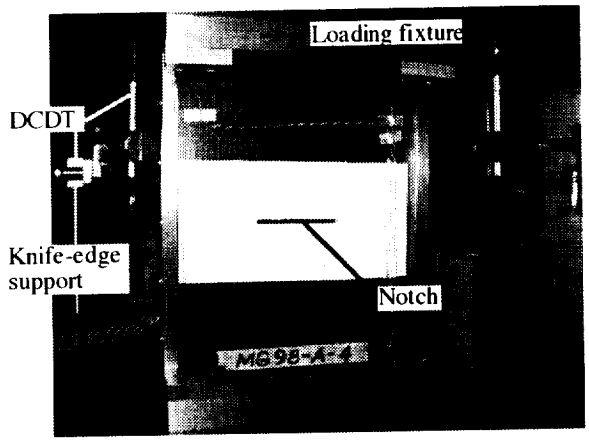

(a) Test setup

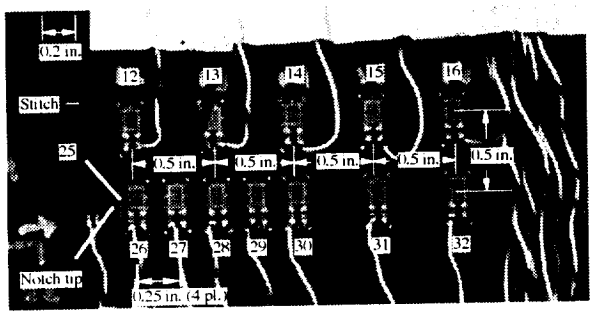

(b) Electrical resistance strain gages used to measure surface strains

Fig. 2. Photographs of plate P-90.

Analysis Procedure

The progressive failure analysis methodology of Ref. 4, as well as the technique used to model damage with superposed shell elements, is described in this section. A discussion of the material strength parameters used in the analysis and descriptions of the finite element models used for the analyses are presented as well.

Progressive Failure Analysis Methodology

Failure modes in laminated composite materials are strongly dependent on geometry, loading direction, and ply orientation. There are four basic failure mechanisms that can induce compression failure in a laminated composite: matrix tensile/compressive cracking, fiber-matrix shearing, fiber buckling, and delamination. The delamination failure mechanism is not included in the present analysis methodology. To predict accurately the damage growth, the failure analysis must be able to predict the failure mode in each ply and apply the corresponding reduction in material stiffness for that ply. The compression failure criteria applied in Ref. 4 as well as the present study are those for unidirectional-fiber composites as proposed by Hashin[5], with the elastic stiffness degradation models developed for compression by Chang et al.[6]. The failure modes considered herein and the failure criteria are summarized below.

Matrix failure in tension and compression occurs due to a combination of transverse stress, σ_y, and shear stress, σ_{xy}. The failure index, e_m, can be defined in terms of these stresses and the strength parameter Y and the shear strength S_c. The matrix strength Y takes the values of Y_t in tension and Y_c in compression. When the failure index exceeds 1.0, failure is assumed to occur. The failure index has the form:

$$e_m^2 = \left(\frac{\sigma_y}{Y_{t/c}}\right)^2 + \left(\frac{\sigma_{xy}}{S_c}\right)^2 \qquad (1)$$

Fiber buckling occurs when the maximum compressive stress in the fiber direction exceeds the fiber buckling strength, X_c, independently of the other stress components:

$$e_b = -\frac{\sigma_x}{X_c} \qquad (2)$$

Fiber-matrix shearing failure occurs due to a combination of fiber compression and matrix shearing. The failure criterion has the form:

$$e_f^2 = \left(\frac{\sigma_x}{X_c}\right)^2 + \left(\frac{\sigma_{xy}}{S_c}\right)^2 \qquad (3)$$

The ply strengths for each ply orientation are presented in Table 2. The strengths reported in this table were obtained by dividing the design allowables in Ref. 7 by 0.85, which is the margin of safety built into the allowables by Boeing.

Table 2. Ply strengths for each ply orientation of the test plates

	Ply orientation		
Strength, ksi	45°	0°	90°
X_t	231	257	213
X_c	175	175	175
S_c	20.6	20.6	20.6
Y_t	5.88	5.88	5.88
Y_c	36.5	36.5	36.5

To simulate the failure modes, the elastic properties are made to be linearly dependent on three field variables, FV1 through FV3. The first field variable represents the matrix failure, the second the fiber-matrix shearing failure, and the third the fiber-buckling failure. The values of the field variables are set to zero in the undamaged state. After a failure index associated with a given failure mode has exceeded 1.0, the associated user-defined field variable is set equal to 1.0. The associated field variable then continues to have the value of 1.0, even though the stresses may decrease significantly. Consequently, the material does not "heal" after it has become damaged. The dependence of the elastic material properties on the field variables is shown in Table 3.

Table 3. Dependence of the elastic material properties on the field variables

Material State	Elastic Properties				FV1	FV2	FV3
No failure	E_1	E_2	ν_{12}	G_{12}	0	0	0
Matrix failure	E_1	0	0	0	1	0	0
Fiber-matrix shear	E_1	E_2	0	0	0	1	0
Fiber buckling	0	0	0	0	0	0	1

Once damage is detected in an element, the mechanical properties in the damaged area are reduced appropriately, according to the property degradation model defined in Table 3. For example, when the matrix failure criterion is exceeded, the field variable *FV1* takes the value of 1, and by the interpolation rule defined in Table 3, the transverse and shear moduli, E_2 and G_{12}, and the Poisson's ratio, υ_{12}, are set to zero. The field variables can be made to transition from 0 (undamaged) to 1 (fully damaged) instantaneously or as any specified function of the failure indices. In the present work, which uses Chang's degradation model, the transition is assumed to be instantaneous. The material degradation model employed herein also attempts to account for the effect of matrix failure by applying a reduction in the fiber-buckling strength for the affected element. This reduction is accomplished by multiplying the fiber-buckling strength by a reduction scale factor, *FBFA*. The effect of varying the value of *FBFA* is studied for plate P-90, and the results will be discussed subsequently.

The finite element implementation of this failure analysis was developed in ABAQUS using the USDFLD user-written subroutine.[8-9] The program calls this routine at all material points of elements whose material properties are defined in terms of the field variables. The routine provides access points to a number of variables such as stresses, strains, material orientation, current load step, and material name, which can be used to compute the field variables. Stresses and strains are calculated at each incremental load step, and evaluated by the failure criteria to determine the occurrence of failure and the mode of failure.

Modeling Damage with Superposed Shell Elements

A progressive damage model for notched laminates under tension was first proposed by Chang et al.[10] The model considers all the possible failure modes in each ply except delamination. Chang et al.[6] later investigated the damage tolerance of composites subjected to compressive loading. The present analysis also deals with compression loads and is largely based on the latter work by Chang. However, the present analysis extends Chang's method from two dimensions to a shell-based analysis that includes bending. Other researchers have performed plate and shell-based progressive failure analyses by applying a material degradation model at every material point in every ply in the laminate.[11-13] In these investigations, the [A,B,D] laminate stiffness matrices are computed from the degraded ply properties. The disadvantage of this method is that the number of material points through the thickness that must be evaluated can be large, even for relatively thin laminates, and can significantly increase the computational effort. For thick laminates such as those described in the present paper, the computational cost of this method may become prohibitive.

To improve the computational efficiency of the analysis, a method based on element superposition was developed in Ref. 4 that separates the failure modes for each ply orientation and does not rely on the computation of the [ABD] matrices. The modeling is done such that the regions ahead of the notch tips, where a potential for damage initiation is anticipated,

are constructed of four superposed layers of shell elements that share the same nodes. No wall offset is applied to any of the elements. Each layer of elements represents one ply orientation (either 0°, 45°, -45° or 90°), and each element spans the entire thickness of the laminate. The implication of this approximation is that the plies for each orientation are uniformly distributed and can be smeared over the thickness of the laminate. Considering that the plates are composed of 10 "stacks" of material (90 plies), this assumption is considered to be adequate. To achieve the correct stiffness, reduced engineering properties are applied to each layer. A reduced material property for a given orientation is simply the product of the engineering property times the sum of the thicknesses of all the plies in that orientation divided by the total thickness of the laminate. Reduced material properties are denoted by the notation $[]_R$., as illustrated in Fig. 3. The elements used in the analyses described herein are the ABAQUS four-node reduced-integration shear deformable elements (S4R, Ref. 8).

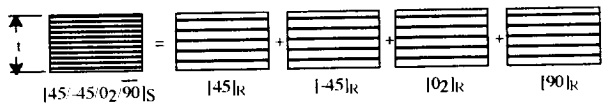

Fig. 3. Thick laminate modeled with four layers of superposed shell elements.

The method of element superposition is convenient for the separation of the failure modes for each ply orientation, and provides the correct membrane and bending stiffnesses. In addition, this separation allows stress and material axes to be defined along the fiber direction, which facilitates the computation of the failure modes in terms of unidirectional material properties.

Material Strength Parameters

As was described previously, the material degradation model applied in this investigation uses failure indices to determine the state of the material. For a particular failure mode and integration point, the state can either be intact or failed, without an intermediate state. The results presented in Ref. 4 indicate that material strength values necessary for optimal correlation with the experimental results were higher than the nominal values by some factor *FA*. This apparent increased strength was attributed to the three factors discussed below.

The first factor is the stabilizing effect that the surrounding material has on the highly loaded fibers in the vicinity of the damage front. This effect results in an increase in the fiber buckling strength. Lessard et al.[14] conducted an analytical investigation of the effect load distribution on the fiber buckling strength of unidirectional composites using an analysis based on an energy principle. Their results showed an increase in the fiber buckling strength of 1.79 for fibers on the hole boundary of a circular cutout as compared to the value calculated for laminates with uniform loading. Chang et al.[6] later used this model to calculate *in situ* fiber buckling strengths for inclusion in their progressive damage model of compression-loaded composite laminates containing open holes.

The second factor contributing to the difference in the apparent material strengths is that some small-scale delamination is undoubtedly taking place, which may cause some local load redistribution and may reduce the local stresses. Such delaminations are not included in the present analysis methodology. The third factor discussed in Ref. 4 is that the analytical model does not include material nonlinearity prior to and during failure.

A fourth factor contributing to the difference in the apparent material strengths is that the *in situ* ply matrix strengths may be much larger than the nominal values obtained using uni-directional laminates. Chang et al.[6] presented an analysis that predicts that the *in situ* tensile and shear strength of unidirectional plies in a laminate can be as much as two times the nominal values. The Chang model accounts for the effect that the ply orientation of the surrounding plies can have on the strength. The effect of laminate stacking sequence is also discussed by Hart-Smith in Ref. 15.

In an attempt to account for the difference in the apparent material strengths, Dávila et al.[4] applied the previously described factor *FA* uniformly to all of the material strengths listed in Table 2. This procedure has been modified in the present analysis to allow different scale factors to be applied to the fiber buckling strength, X_c, and the three matrix strengths, Y_t, Y_c, and S_c. The scale factors applied to the fiber buckling strength and the matrix strengths are *FAF* and *FAM*, respectively. The matrix strength scale factor *FAM* is included as a separate parameter to allow for an investigation of the effect of the matrix strength on the analytical results. As mentioned previously, there can be a significant difference between the nominal matrix strength obtained using uni-directional laminates and the *in situ* matrix strength. Hart-Smith discusses a laminate stacking sequence effect that can have a significant impact on matrix cracking. This effect results from an interaction with adjacent plies that can act as crack stoppers.[15]

Dávila et al.[4] also applied a stitching scale factor, *SF*, to the fiber buckling strength in the rows of elements located in the anticipated failure path that correspond to the location of the stitches. This scale factor was only applied to the 0-degree plies of the elements coinciding

with the locations of the stitch lines, and it was used to account for the local reinforcing effect of the stitches that resulted in discrete growths in the length of the damage zone. These discrete growths in damage were determined in Ref. 4 to coincide with the locations of the stitch lines. Results illustrating the effect of varying these scale factors are discussed subsequently.

Finite Element Models

The analytical results described in the present paper were obtained from nonlinear analyses performed using the ABAQUS finite element code.[8] The finite element model used in the analysis of panel P-90 is shown in Fig. 4(a). A quarter-panel model was used since symmetry lines exist in the structure. A close-up view of this model near the notch tip shown in Fig. 4(b).

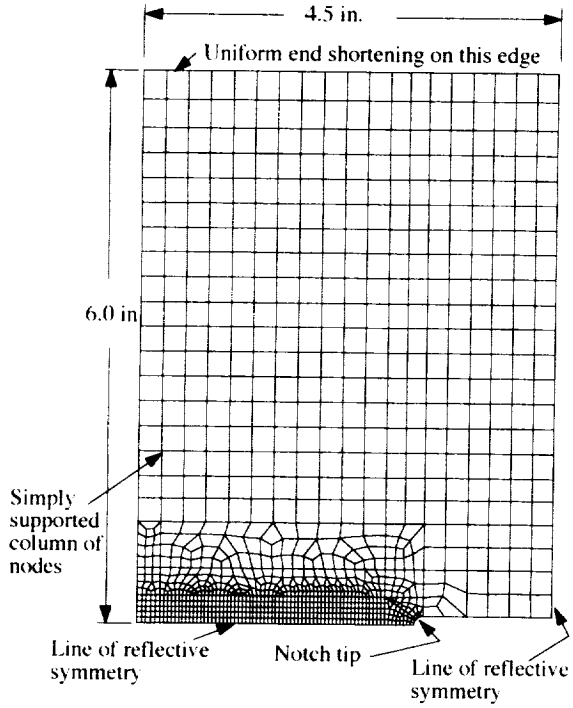

(a) Full model

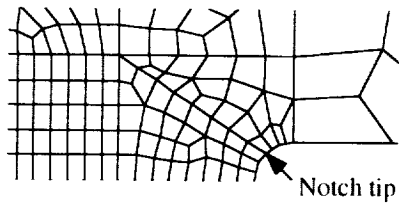

(b) Close up of mesh at notch tip

Fig. 4. Finite element model of panel P-90.

The finite element mesh is much more refined near the notch tip to allow for an accurate representation of the strain field in the vicinity of the notch tip and in the anticipated path of damage growth. The finite element model used in the analysis of panel P-60 is shown in Fig. 5(a). A close-up view of this model near the notch tip is shown in Fig. 5(b). The discretization of the finite element model of panel P-45 is very similar to that used for panel P-60. The elastic material properties used in the analyses are given in Table 1. The numbers of nodes, elements, and active degrees of freedom for each finite element model are summarized in Table 4.

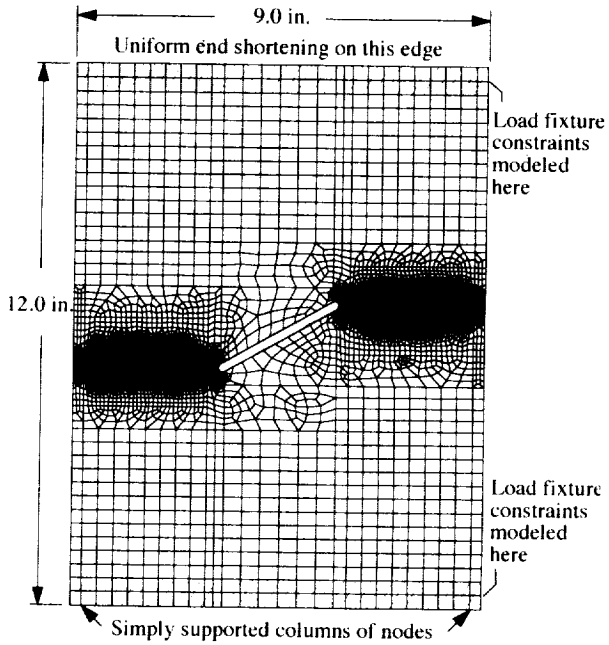

(a) Full model

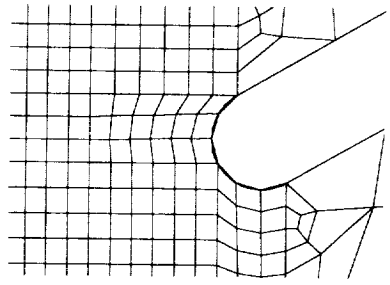

(b) Close up of mesh at notch tip

Fig. 5. Finite element model of panel P-60.

Table 4. Summary of finite element model information

Panel model	Number of nodes	Number of elements	Active DOF
P-90	1109	2151	6654
P-60	5800	13876	34800
P-45	5627	12090	33762

Results and Discussion

Results from the compression tests and analyses of the three notched composite plates are described in this section. A discussion of the effects of the scale factors described previously is presented. These scale factors are *FAF* (applied to the fiber-buckling strength), *FAM* (applied to the matrix strengths), *SF* (the stitching scale factor) and *FBFA* (the fiber-buckling-strength reduction factor). Comparisons of displacements and strains obtained from the experiments and analyses are presented and compared for each plate.

Panel P-90

The reaction force for plate P-90 is shown as a function of the applied end-shortening displacement in Fig. 6 for three different values of the fiber-buckling-strength scale factor *FAF*. The convention used for this and all subsequent figures is to show the results obtained from the experiment as open symbols and results obtained from the analyses as filled symbols. The value of *FAM* for the analyses used to obtain these results was 1.0 (i.e., nominal values used for the matrix strengths), while the values of the stitching scale factor *SF* and the fiber-buckling-strength reduction scale factor *FBFA* were 1.7 and 0.1, respectively. The results shown in Fig. 6 indicate that optimal correlation is obtained for a value *FAF* = 1.52.

This result for the optimal value of *FAF* is consistent with the results shown in Fig. 7. The values of strain at the location of strain gage 12 (see Fig. 2(b)) are shown in this figure as a function of the applied end-shortening displacement. Gage 12 was selected because it is not in the damage path, and would therefore provide information throughout the entire loading of the plate. Results obtained using a value of *FAF* = 1.52 provides excellent correlation with the experimental results, as shown in Fig. 7. Note that the analytical results capture the sudden decrease in strain at gage 12 as the damage front approaches its location. These results indicate that the *in situ* value of the fiber buckling strength is 1.52 times the nominal value. A value of 1.52 will therefore be used for all subsequent analyses of plate P-90. This value of FAF is consistent with those reported by Lessard et al.[6] (1.79) and Dávila et al.[4] (1.25 – 1.60).

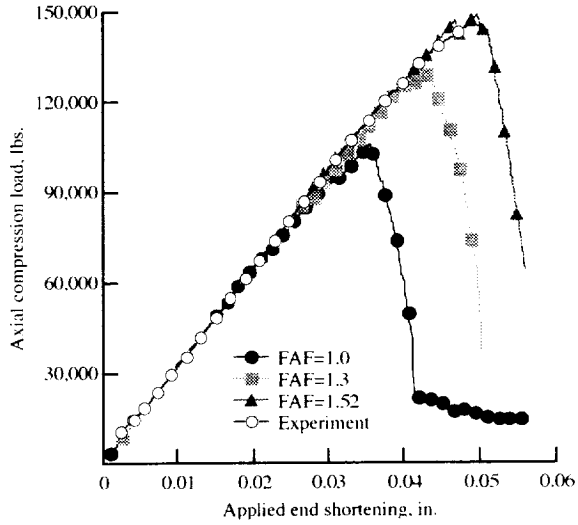

Fig. 6. Reaction force as a function of the applied end-shortening displacements for plate P-90.

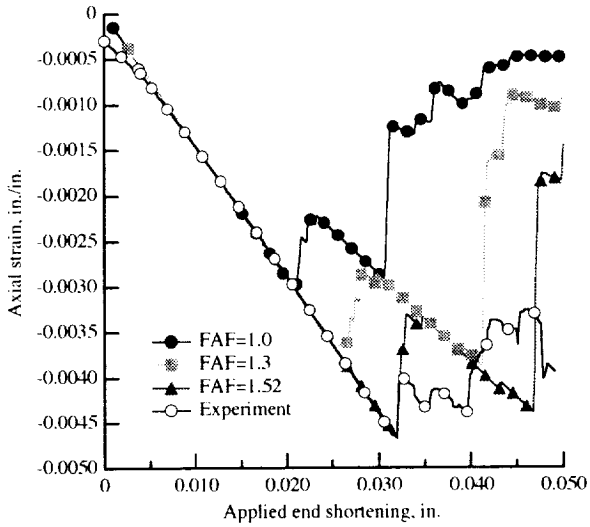

Fig. 7. Axial strains at strain gage 12 location for plate P-90 (see Fig. 2(b)).

The reaction force for plate P-90 is shown as a function of the applied end-shortening displacement in Fig. 8 for plate P-90 for three values of the stitching scale factor *SF*. The value of *FAF* used to obtain these results was 1.52, while the values of matrix-strength scale factor *FAM* and the fiber-buckling-strength reduction scale factor *FBFA* were 1.0 and 0.1, respectively. The results shown in Fig. 8 indicate that optimal correlation is obtained for a value *SF* equal to 1.7. This value is approximately 26 percent lower than the value of 2.3 used in Ref. 4. The difference in the values used for each study is attributed to the

differences in manufacturing methods, including stitching machines.

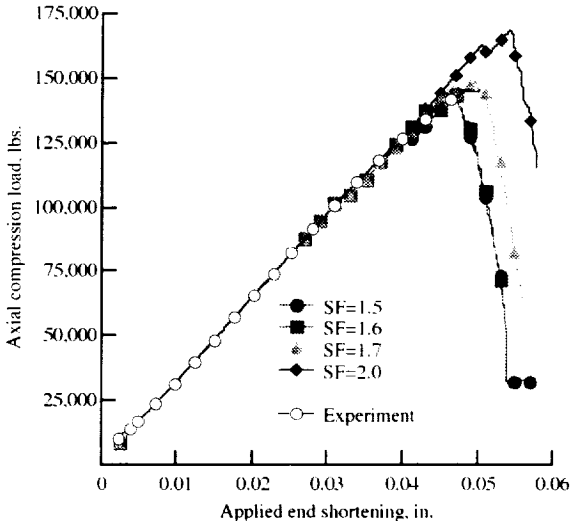

Fig. 8. Reaction force as a function of the applied end-shortening displacements for plate P-90.

The optimal value of the stitch factor *SF* is consistent with the results shown in Fig. 9. The values of strain at the location of strain gage 12 (see Fig. 2(b)) are shown in this figure as a function of the applied end-shortening displacement. As shown in Fig. 7, the predicted strains obtained using a value of $SF = 1.7$ provide excellent correlation with the measured strains. Note that the analytical results for vales of *SF* of 1.6 and 1.7 capture the sudden decrease in strain at gage 12 as the damage front approaches its location. However, better overall correlation with the final failure load is obtained by using $SF = 1.7$. These results indicate that the effect of the stitching on the local *in situ* value of the fiber buckling strength in the 0-degree plies is to increase the nominal value by 70 percent compared to the unstitched material. Note that the factor *SF* is applied in addition to the factor *FAF* only for the 0-degree plies in the locations that correspond to the stitch locations. A value of $SF = 1.7$ will be used for all subsequent analyses of plate P-90.

The reaction force for plate P-90 is shown as a function of the applied end-shortening displacement in Fig. 10 for three values of the fiber-buckling-strength reduction scale factor *FBFA*. This scale factor is used to reduce the fiber buckling strength in the presence of matrix failure. The value of *FAF* for the analyses used to obtain these results was 1.52, while the values of *FAM* and *SF* were 1.0 and 1.7, respectively.

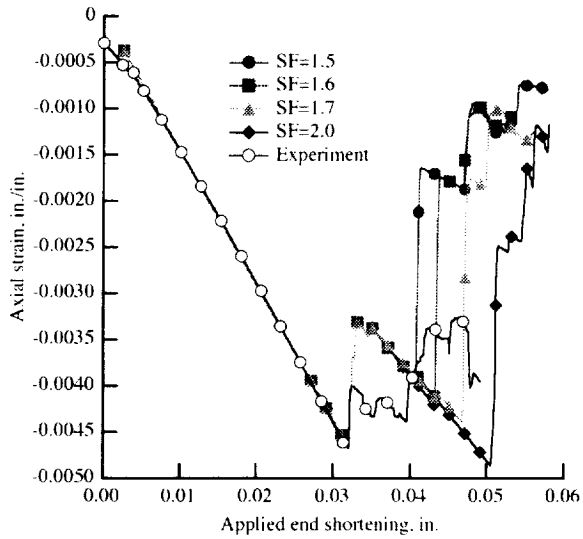

Fig. 9. Axial strains at strain gage 12 location for plate P-90 (see Fig. 2(b)).

In Fig. 10, a value of $FBFA = 0.1$ corresponds to a reduction in the fiber buckling strength of 90 percent relative to the nominal value. The results shown in Fig. 10 indicate that the value of this factor has a negligible effect on the results obtained from the analysis. The correlation of the analytical results with the experimental results is slightly better when a value of $FBFA = 0.1$ is used. The results for the location of strain gage 12 that are shown in Fig. 11 confirm this result. Therefore, a value of $FBFA = 0.1$ will be used in all subsequent analyses of plate P-90.

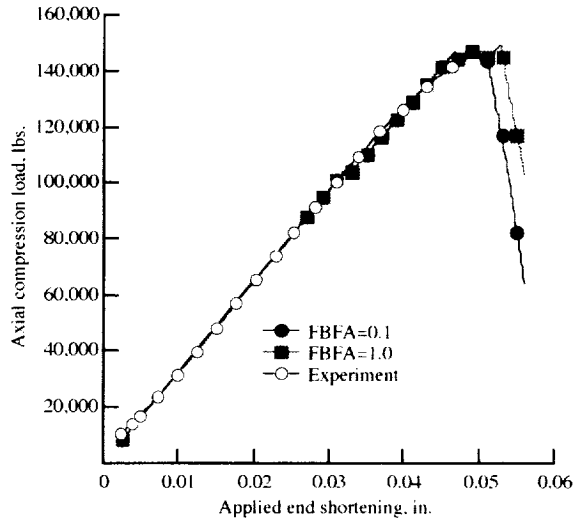

Fig. 10. Reaction force as a function of the applied end-shortening displacements for plate P-90.

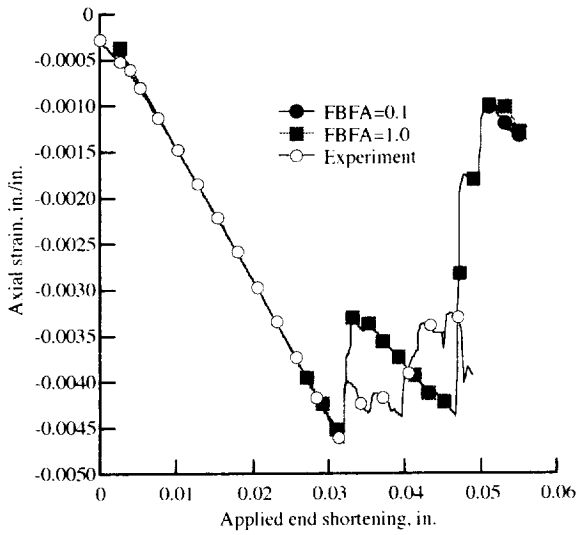

Fig. 11. Axial strains at strain gage 12 location for plate P-90 (see Fig. 2(b)).

The reaction force for plate P-90 is shown in Fig. 12 as a function of the applied end-shortening displacement for plate P-90 for three values of the matrix-strength scale factor *FAM*. The value of *FAF* for the analyses used to obtain these results was 1.52, while the values of *SF* and *FBFA* were 1.7 and 0.1, respectively. The results shown in Fig. 12 indicate that the value of this factor has very little effect on the results obtained from the analysis for values of *FAM* = 1.0 and 1.25. A more appreciable effect occurs for *FAM* = 1.5. However, the correlation between the analytical and experimental results for this value is inferior to that for the other two values considered.

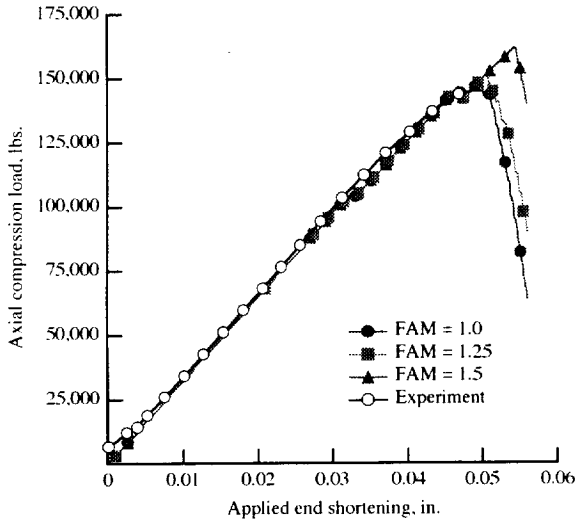

Fig. 12. Reaction force as a function of the applied end-shortening displacements for plate P-90.

The results for the location of strain gage 12 that are presented in Fig. 13 confirm this result. The results for this configuration are relatively insensitive to increases in the material allowable values of amounts up to 50 percent. Note that the results presented in Fig. 7 and Fig. 13 indicate that the fiber-buckling strength scale factor *FAF* is the most important parameter in predicting the first occurrence of damage in this panel. The results in Fig. 7 indicate that a value of *FAF* = 1.52 is required to predict accurately the first occurrence of damage at the location of strain gage 12. Furthermore, the results presented in Fig. 13 indicate that this prediction of the first occurrence of damage is not sensitive to changes in the value of *FAM*. This result can not necessarily be extrapolated to plates P-60 and P-45, since the increased levels of shear stresses present at the notch tip can be expected to affect this result. This effect was examined for plate P-60. The results of those analyses, which are presented subsequently, confirmed that a value of *FAM* = 1.25 provided good correlation between the analytical and experimental results. Therefore, a value of *FAM* = 1.25 was selected for use in all subsequent analyses of plate P-90.

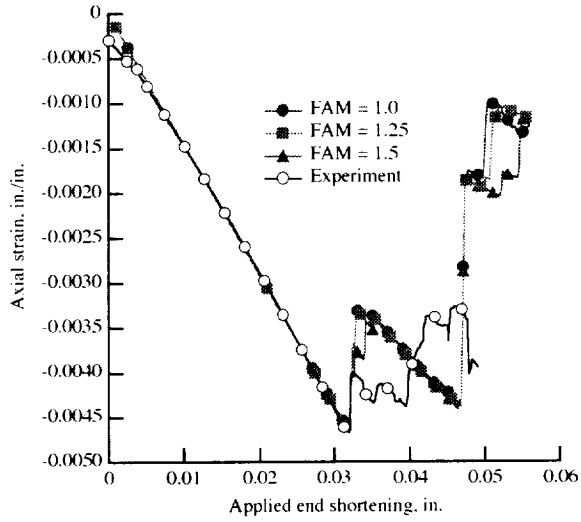

Fig. 13. Axial strains at strain gage 12 location for plate P-90 (see Fig. 2(b)).

The four strain gages whose results are shown in Fig. 14 were placed on plate P-90 in the vicinity of the notch tip to monitor the growth of the damage zone. The locations of these gages are shown in Fig. 2(b). Gages G25 and G28 are in the path of the damage. Gages G12 and G13 are not in the damage path, but gage G13 is in the load path of gage G28. The experimental results shown in Fig. 14(a) indicate that damage initiation occurred at an applied end shortening displacement of 0.032 in (point A in Fig. 14(a)). The results shown in this figure indicate that the damage zone grew into the

area of gage G25, as evidenced by the large change in the measured strain value. This damage growth is confirmed by the data from gage G12, which indicates a reduction in the load as a consequence of the damage propagation. Small increases in negative strains are also noted in gages G28 and G13, indicating that load redistribution has occurred. No further damage is measured until an end shortening displacement of 0.0478 inches (point B in Fig. 14(a)), when damage growth is indicated again through a large change in measured strain at gages G13 and G28. Final failure of the panel occurs soon after this point at a value of applied end shortening of 0.0491 inches and an applied load of 145.2 kips.

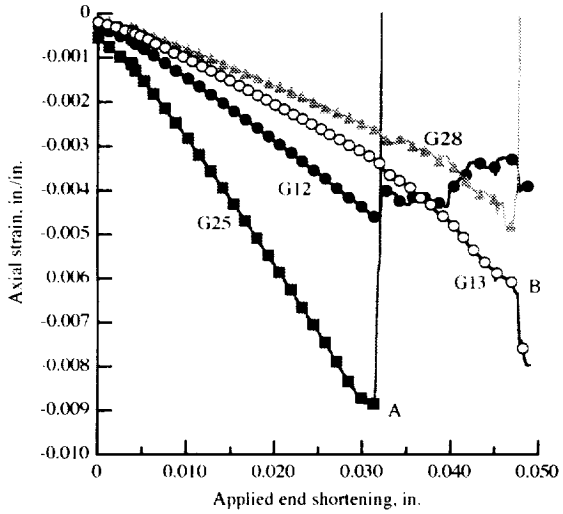

(a) Measured strains

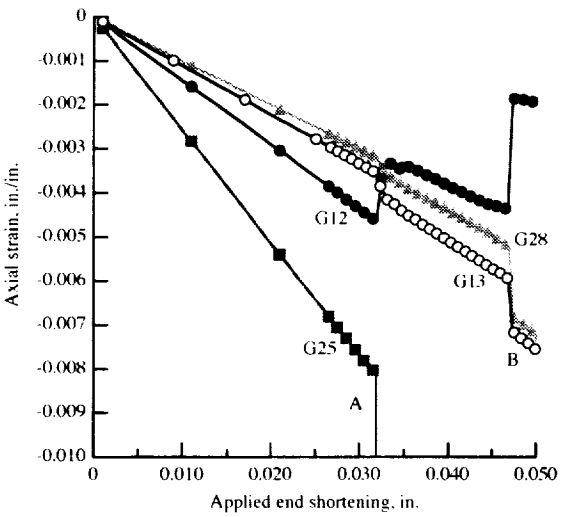

(b) Computed strains

Fig. 14. Measured and computed strains for gages 12, 13, 25, and 28 for plate P-90 (see Fig. 2(b)).

The analytical model presented in Ref. 4, was used to determine that the reason for the discrete increments in damage growth is that the stitch lines increase locally the fiber buckling strength by tying all the plies in the laminate together. For this panel, the stitch lines run perpendicular to the notch direction and have a spacing of approximately 0.2 inches, as can be seen in the photograph of Fig. 2(b).

The finite element analysis results shown in Fig. 14(b) have the same characteristics as the test results shown in Fig. 14(a). These characteristics are discrete damage growth at applied end-shortening displacements of 0.0320 and 0.0470 inches (points A and B, respectively, in Fig. 14), and predicted failure of the panel at an applied end-shortening of 0.0507 inches and a value of the reaction force of 151.1 kips. The predicted values of end shortening and reaction force at failure differ from the experimental results by 3.26 and 4.1 percent, respectively. The predicted unloading response of gage G12 and load redistribution responses at gages G13 and G28 are accurate throughout the loading range considered. Note that the change of sign in the measured strain at gages G25 and G13 (see Fig. 14(a)) is attributed to local delaminations at the gage location that resulted in large local bending of the outer surface plies. The values of the scale factors used in the analysis to generate these results were $FAF = 1.52$, $SF = 1.7$, $FAM = 1.25$, and $FBFA = 0.1$.

Photographs of plate P-90 after failure are shown in Fig. 15. The damage propagated across the width of the panel, and the panel failed at a load of 145.2 kips.

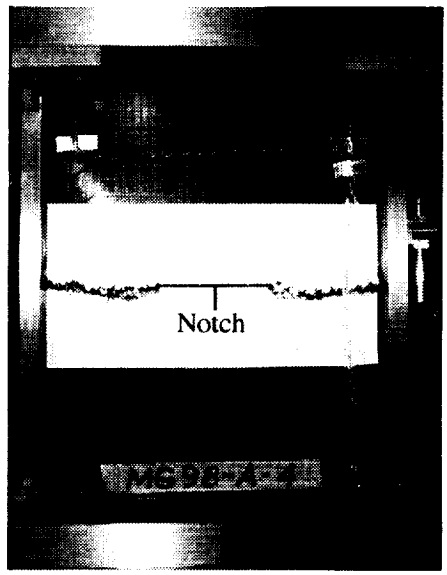

(a) Failure mode as viewed from the front of the plate

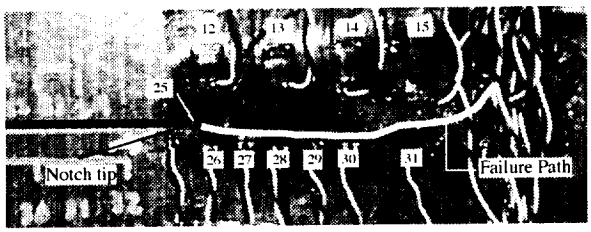

(b) Detailed view of the failure mode as viewed from the back surface of the plate

Fig. 15. Failure mode for plate P-90.

The distributions of the failure modes ahead of the notch tip are shown in Fig. 16 for the three-ply orientations of 0, 45, and 90 degrees, at an applied end-shortening displacement of 0.0507 inches. The corresponding reaction force is 151.1 kips. Dark-colored elements are designated as failed by the analysis for a particular mode and ply orientation. The fiber-shear and fiber buckling failure modes are the dominant failure modes in the 0-degree plies and the matrix failure mode dominates in the 45- and 90-degree plies.

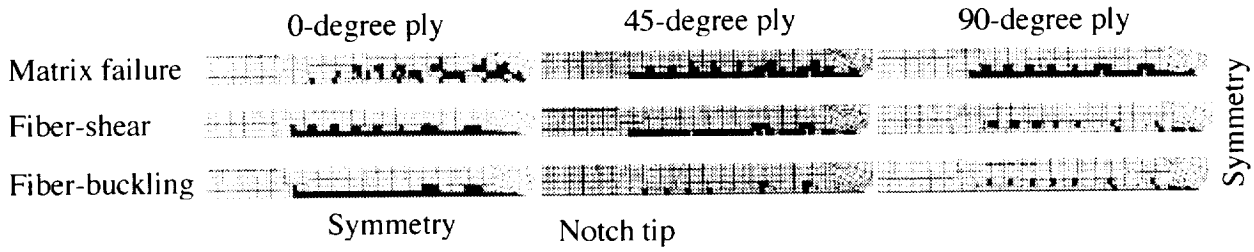

Fig. 16. Distribution of failures by mode and ply orientation for plate P-90 for an end-shortening displacement of 0.0507 inches.

Panel P-60

The reaction force for plate P-60 is shown as a function of the applied end-shortening displacement in Fig. 17 for four different values of the fiber-buckling-strength scale factor *FAF*. Except where noted in the figure, the value of *FAM* for the analyses used to obtain these results was 1.5, while the values of *SF* and *FBFA* were 1.7 and 0.1, respectively. The results shown in Fig. 17 indicate that optimal correlation is obtained for a value *FAF* equal to 1.8. Due to a data acquisition system error, no experimental data is available for axial compression loads greater than 139 kips or applied end shortening displacements greater than 0.043 in. However, the final failure load of plate P-60 was 155 kips. This data point is indicated in Fig. 17 by linearly extrapolating the experimental results to a value of 155 kips. This extrapolation is considered to reasonable since the amount of progressive damage growth prior to failure of the panel was small.

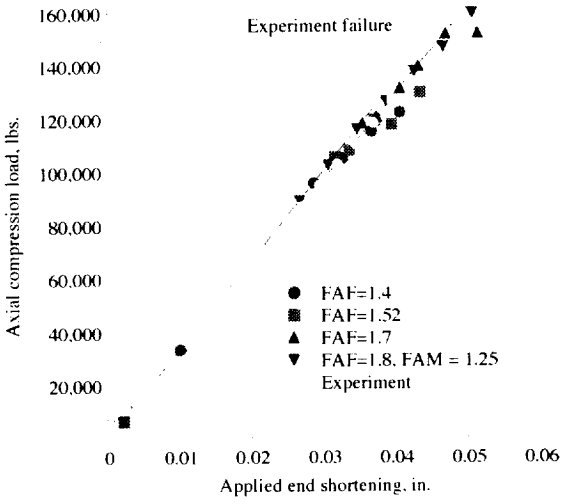

Fig. 17. Reaction force as a function of the applied end-shortening displacements for plate P-60.

This result for the optimal value of *FAF* is consistent with the results shown in Fig. 18. The values of strain at the location of strain gage 13 (see Fig. 19) are shown in this figure as a function of the applied end-shortening displacement. As shown in Fig. 18, the results obtained using a value of *FAF* = 1.8 provide excellent correlation with the experimental results. Note that the analytical results capture the sudden change in the strain reading at gage 13 as the damage front approaches its location. These results indicate that the *in situ* value of the fiber buckling allowable is 1.8 times the nominal value. A value of 1.8 will therefore be used for all subsequent analyses of plate P-60.

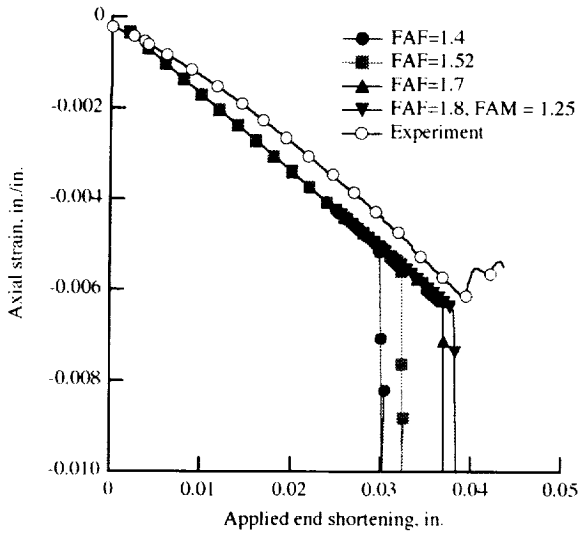

Fig. 18. Axial strains at strain gage 13 location for plate P-60 (see Fig. 19).

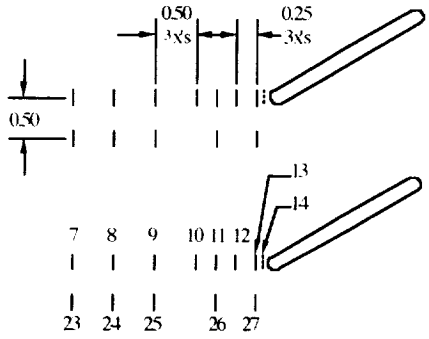

Fig. 19. Location of strain gages in the vicinity of the notch tip for plates P-60 and P-45.

The reaction force for plate P-60 is shown as a function of the applied end-shortening displacement in Fig. 20 for three values of the scale factor *FAM*. Except where noted in the figure, the value of *FAF* for the analyses used to obtain these results were 1.7, while the values of *SF* and *FBFA* were 1.7 and 0.1, respectively. The results shown in Fig. 20 indicate that changing the value of *FAM* from 1.0 to 1.25 has a large effect on the results. However, the effect of changing *FAM* from 1.25 to 1.5 is negligible. The correlation between the analytical and experimental results for values of FAM of 1.25 and 1.5 is excellent.

The values of strain at the location of strain gage 13 (see Fig. 19) are shown in Fig. 21 as a function of the applied end-shortening displacement. These results indicate that the strain results for this configuration are relatively insensitive to increases in the value of *FAM* by up to 25 percent. However, a change of 50 percent(i.e., FAM = 1.5) does produce a change in the

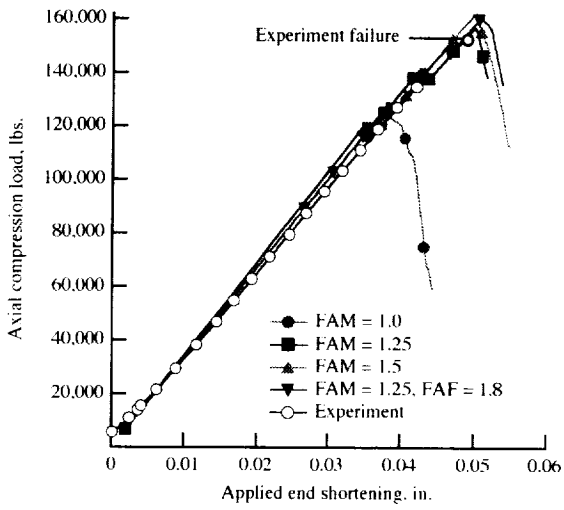

Fig. 20. Reaction force as a function of the applied end-shortening displacements for plate P-60.

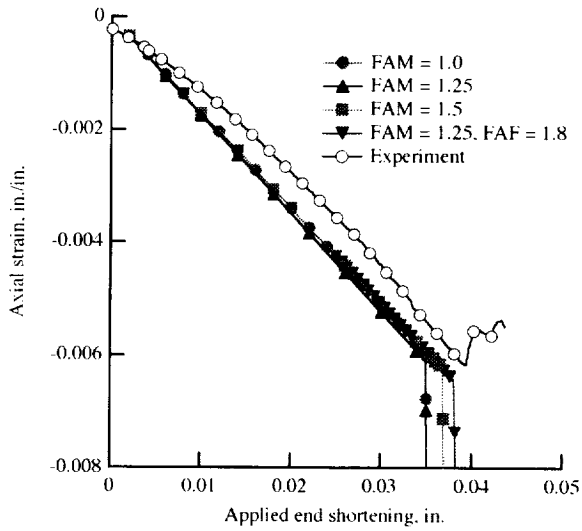

Fig. 21. Axial strains at strain gage 13 location for plate P-60 (see Fig. 19).

prediction of damage initiation at this location. However, the fiber-buckling-strength scale factor FAF is considered to be the dominant parameter since a change in this value from 1.7 to 1.8 (5 percent) results in better correlation with the experimental results, as shown in Fig. 21.

The five strain gages whose results are shown in Fig. 22 were placed on plate P-60 in the vicinity of the notch tip to monitor the growth of the damage zone. The locations of these gages are shown in Fig. 19. Gages G14, G13, and G11 are in the path of the damage.

Gages G27 is in the load path of gage G13 and gage G26 is in the load path of gage G11. The experimental results shown in Fig. 22(a) indicate that damage initiation occurred at an applied end-shortening displacement of 0.0394 in. (point A in Fig. 22(a)). The results shown in this figure indicate that the damage zone grew into the area of gages G14 and G13, as evidenced by the large change in measured strain values. Experimental data is not available past values of the applied end-shortening displacement of 0.0435 in. The final failure load of plate P-60 was 155.0 kips.

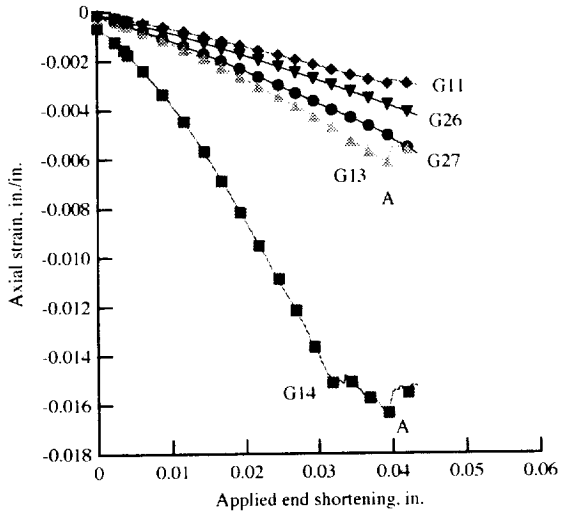

(a) Measured strains

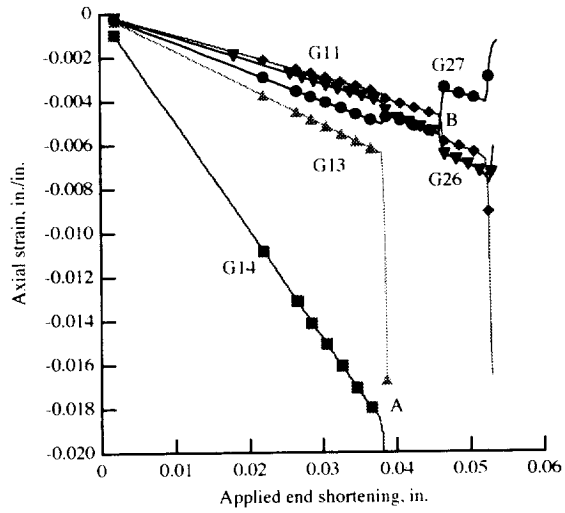

(b) Computed strains

Fig. 22. Measured and computed strains for gages 11, 13, 14, 26, and 27 for plate P-60 (see Fig. 19).

The finite element analysis results shown in Fig. 22(b) accurately predict the first occurrence of damage in plate P-60. There is discrete damage growth predicted at an applied end shortening displacement of 0.0384 in. (point A in Fig. 22(b)). This analysis also predicts accurately the maximum value of the reaction force of 161.2 kips at an applied end-shortening displacement of 0.051 inches. The predicted value of reaction force at failure differs from the experimental result by 4.0 percent. The values of the various scale factors used in the analysis to generate these results were $FAF = 1.8$, $SF = 1.7$, $FAM = 1.25$, and $FBFA = 0.1$.

Panel P-45

The five strain gages whose results are shown in Fig. 23 were placed on plate P-45 in the vicinity of the notch tip to monitor the growth of the damage zone. The locations of these gages are shown in Fig. 19. Gages G14, G13, and G11 are in the path of the damage. Gages G27 is in the load path of gage G13 and gage G26 is in the load path of gage G11. The experimental results shown in Fig. 23(a) indicate that damage initiation occurred at an applied end-shortening displacement of 0.0405 in. (point A in Fig. 23(a)). The results shown in this figure indicate that the damage zone grew into the area of gages G14 and G13, as evidenced by the large change in measured strain values. This damage growth is confirmed by the data from gage G27, which indicates a reduction in the load as a consequence of the damage propagation. Small increases in negative strains are also noted in gages G11 and G26, indicating that load redistribution has occurred. No further damage is measured until an end-shortening displacement of 0.0513 in. (point B in Fig. 23(a)), when damage growth is indicated again through a large change in measured strain at gages G11 and G27. Reaction force data indicate that the plate supports the largest reaction force of 161.2 kips at a value of applied end shortening of 0.0524 just prior to final failure. The final failure of the panel occurs soon after this point at a value of applied end shortening of 0.0541 inches and a reaction force of 157.9 kips.

The finite element analysis results shown in Fig. 23(b) have the same characteristics as the test results. These characteristics are discrete damage growth at applied end-shortening displacements of 0.039 and 0.0512 in. (points A and B, respectively, in Fig. 23(b)), and predicted failure of the panel at an applied end-shortening of 0.0512 inches and a maximum value of the reaction force of 172.2 kips. The predicted values of end shortening and reaction force at failure differ from the experimental results by 1.53 and 6.82 percent, respectively. The predicted unloading response of gage G27 and load redistribution responses at gages G11 and G26 are accurate throughout the loading range

considered. The values of the various scale factors used in the analysis to generate these results were *FAF* = 1.8, *SF* = 1.7, *FAM* = 1.25, and *FBFA* = 0.1.

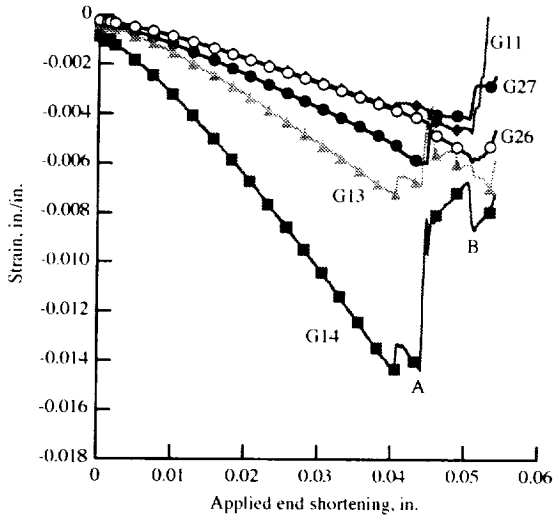

(a) Measured strains

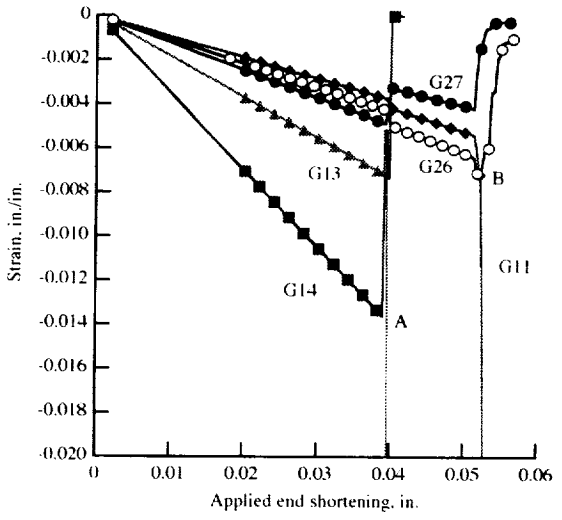

(b) Computed strains

Fig. 23. Measured and computed strains for gages 11, 13, 14, 26, and 27 for plate P-45 (see Fig. 19).

Note that the only scale factor whose value was changed for the final analysis of each of the plates was *FAF*. A value of FAF = 1.52 was used for plate P-90, and a value of FAF = 1.8 was used for plates P-60 and P-45. The average value of *FAF* is 1.71. The values of the other scale factors used for all three plates were *SF* = 1.7, *FAM* = 1.25, and *FBFA* = 0.1.

Concluding Remarks

The results of an experimental and analytical evaluation of damage progression in three stitched composite plates containing a central notch that is oriented at an angle α to the direction of the applied uniaxial compression loading were presented. The values of α considered in the present study are 45°, 60°, and 90°. The progressive failure analysis methodology used was a modified version of a previously developed method that was utilized for the step-by-step simulation of damage growth in large stiffened stitched composite wingbox cover panels. Three failure indices corresponding to all the major failure modes except delamination were used to evaluate the modes of failure, and their location. Superposed layers of shell elements with multiple integration points through the thickness were used to separate the failure modes for each ply orientation and to obtain the correct effect of bending loads on damage progression. All the plies in any particular orientation were smeared together and combined into one shell element. This method of superposition avoids the computational expense associated with the otherwise necessary process of evaluating the failure criteria at every integration point in every ply. This methodology was implemented into the ABAQUS finite element code.

Parametric studies of several important material parameters were conducted to identify appropriate *in situ* values to be included in the progressive failure analyses of the three plates. These parametric studies indicate that the *in situ* value of the fiber buckling strength is the most important parameter in the prediction of damage initiation and growth in these notched composite plates subjected to compression loading.

Three plates with different notch orientations were tested and analyzed using *in situ* material strength values in this investigation. The strains, reaction loads, and damage growth histories were predicted and found to agree with the experimental results to within seven percent. The stitching in the plates was found to retard the growth of damage by delaying the onset of fiber buckling in the 0-degree plies. The stitching and the thickness of the laminates probably contributed to the accuracy of the solution by nearly eliminating delamination as one of the damage modes in the plates.

References

[1]Markus, A., Thrash, P., and Grossheim, B., "Manufacturing Development and Requirements for Stitched/RTM Wing Structure," Proceedings of the Fourth NASA/DoD Advanced Composites Technology Conference, NASA CP 3229, 1993, pp. 503-523.

[2]Karal, M., "AST Composite Wing Program – Executive Summary," NASA CR 2001-210650.

[3]Jegley, D. C., and Bush, H. G., "Structural Test Documentation and Results for the McDonnell Douglas All-Composite Wing Stub Box," NASA TM 110204, April 1997.

[4]Dávila, C. G., Ambur, D. R., and McGowan, D. M., "Analytical Prediction of Damage Growth in Notched Composite Panels Loaded in Axial Compression," *Journal of Aircraft*, Vol. 37, No. 5, Sept.-Oct. 2000.

[5]Hashin, Z., "Failure Criteria for Unidirectional Fiber Composites," *Journal of Applied Mechanics*, Vol. 47, 1980, pp. 329-334.

[6]Chang, F. K., and Lessard, L. B., "Damage Tolerance of Laminated Composites Containing an Open Hole and Subjected to Compressive Loadings: Part I-Analysis," *Journal of Composite Materials*, Vol. 25, 1991, pp. 2-43.

[7]Hinrichs, S., General Methods for Determining Stitched Composite Material Stiffnesses and Allowable Strengths, Vol. 1, McDonnell Douglas Report No. MDC94K9113, March 1995.

[8]Anon., ABAQUS User's Manual, Vol. III, Version 5.6, Hibbitt, Karlsson & Sorensen, Pawtucket, RI, pg. 25.2.33-1, 1996.

[9]Anon., ABAQUS Example Problems Manual, Vol. I, Version 5.5, Hibbitt, Karlsson & Sorensen, Pawtucket, RI, pg. 3.2.25.25-1. 1995.

[10]Chang, F. K., and Chang, K. Y., "A Progressive Damage Model for Laminated Composites Containing Stress Concentrations," *Journal of Composite Materials*, Vol. 21, September 1987, pp. 834-855.

[11]Moas, E., "Progressive Failure Analysis of Laminated Composite Structures," Ph.D. Dissertation, Virginia Polytechnic Institute and State University, Blacksburg, VA, 1996.

[12]Averill, R. C., "A Micromechanics-Based Progressive Failure Model for Laminated Composite Structures," AIAA/ASME/ASCE/AHS/ASC 33rd Structures, Structural Dynamics and Materials Conference, Dallas, Texas, April 13-15, 1992, pp. 2898-2904.

[13]Sleight, D. W., Knight, N. F., Jr., and Wang, J. T., "Evaluation of a Progressive Failure Analysis Methodology for Laminated Composite Structures," 38th AIAA/ASME/ASCE/ASC Structures, Structural Dynamics, and Materials Conference, Kissimmee, FL, AIAA Paper No. 97-1187, April 7-10, 1997.

[14]Lessard, L. B., and Chang, F. K., "Effect of Load Distribution on the Fiber Buckling Strength of Unidirectional Composites," *Journal of Composite Materials*, Vol. 25, No. 1, 1991, pp. 65-87.

[15]Hart-Smith, L. J., "A Re-Examination Of The Analysis Of In-Plane Matrix Failures In Fibrous Composite Laminates," *Composites Science and Technology*, Vol. 56, 1996, pp. 107-121.